Received: 19 January 2019 | Revised: 13 November 2019 | Accepted: 22 November 2019 | Published on: 14 December 2019

DOI: 10.1002/joc.6416

RESEARCH ARTICLE

International Journal of Climatology RMetS

# Automatic identification and classification of the northern part of the Red Sea trough and its application for climatological analysis

**Hadas Saaroni**[1] | **Tzvi Harpaz**[1,2] | **Pinhas Alpert**[3] | **Baruch Ziv**[2]

[1]Department of Geography and the Human Environment, The Porter School of the Environment and Earth Sciences, Tel Aviv University, Tel Aviv, Israel

[2]Department of Natural Sciences, The Open University of Israel, Ra'anana, Israel

[3]Department of Geophysics, The Porter School of the Environment and Earth Sciences, Tel Aviv University, Tel Aviv, Israel

**Correspondence**
Hadas Saaroni, Department of Geography and the Human Environment, The Porter School of the Environment and Earth Sciences, Tel Aviv University, Tel Aviv, Israel.
Email: saaroni@tauex.tau.ac.il

**Funding information**
Israeli Science Foundation, Grant/Award Number: 1123/17

**Abstract**

The Red Sea trough (RST) is a low-pressure trough extending from south towards the Levant. Unlike previous synoptic classifications covering all systems that affect the region, our algorithm focuses on the RST alone. It uses sea-level pressure (SLP) and relative geostrophic vorticity for identifying the existence of an RST and classifying it to one of three types, according to the location of the trough axis with respect to 35°E longitude. The following conditions were imposed to assure the existence of an RST: (a) north to south SLP drop across the Levant, (b) average positive sea-level relative vorticity over the region of interest, (c) existence of a distinct and continuous trough axis from the south towards the region of interest and (d) absence of any pronounced closed cyclone near the Levant. The algorithm was applied on the NCEP/NCAR reanalysis, $2.5° \times 2.5°$ resolution and the ERA-Interim, $2.5° \times 2.5°$ and $0.75° \times 0.75°$ resolutions. An evaluation of the algorithm against subjective identification, based on the NCEP reanalysis, showed an agreement of 93% for RST identification and 79% for correct classification. The use of fine resolution data may insert noise that reduce the identification rate of RSTs but improves the axis locating. The autumn is the main season of RST, with a maximum in November and a consistent decrease towards the July minimum. The annual frequency varies among the data sources between 17.6 and 24.6%. The trough axis is shown to have a diurnal oscillation; towards the eastern coast of the Mediterranean at nighttime and eastward, inland, at noontime. No consistent long-term trend was found for the period 1979–2016, during which the global warming was persistent. This automated algorithm is flexible in the sense that it is not confined to any predetermined spatial resolution and is applicable to operational forecast model as well as to climate model outputs.

KEYWORDS

automatic identification, diurnal variation, Levant, Red Sea trough, synoptic classification, trough axis

  

# 1 | INTRODUCTION

The Red Sea trough (RST) is a low-pressure trough, originating mostly from the "Sudan Monsoon Low," being a part of the equatorial low-pressure thermal system (El-Fandy, 1950; Solot, 1950; Awad and Almazroui, 2016; Awad and Mashat, 2019). The synoptic classification of the RST over the Levant region (Alpert *et al.*, 2004a; Tsvieli and Zangvil, 2005) did not account for the southernmost source of this trough, but confined their analysis to troughs that extend from the middle of the Red Sea. When easterly flow dominates the northern part of the Red Sea, this trough tends to develop northward, along the lee of the continuous mountain ridges, down to the Eastern Mediterranean (EM) and the Levant (e.g., Ashbel, 1938; El-Fandy, 1948; Krichak *et al.*, 1997a, 1997b; Kahana et al., 2002; Alpert *et al.*, 2004a; Tsvieli and Zangvil, 2005). The effectiveness of the topography depends on the structure of both the mid-level westerlies and the lower-level easterlies (Krichak *et al.*, 1997a). Unlike the migratory cyclones that affect the Levant region (the Cyprus and the North African Lows, Alpert and Ziv, 1989; Romem *et al.*, 2007), the RST tends to be quasi-stationary (Saaroni *et al.*, 1996; Ziv *et al.*, 2005; Tsvieli and Zangvil, 2007).

The RST is present during ~20% of the days annually: mostly in the fall, slightly less during the winter, and fades out during the spring (based on the daily definition according the semi-objective synoptic classification of Alpert *et al.* (2004a) for the 1948–2000 period, see Table I in Alpert *et al.* (2004a). Nevertheless, Alpert *et al.* (2004a, in fig. 2a and Table I) show a considerable increase in the frequency of RSTs from 1960 to 2000.

The RST mostly transports hot and dry air from the Arabian Peninsula and surroundings, including Jordan, Syria and Iraq, towards the Levant, via southeasterly low-level winds, often accompanied by haze or dust storms (Dayan *et al.*, 2008; Enzel *et al.*, 2008; Ganor *et al.*, 2010a, 2010b; Erel *et al.*, 2013; Gasch *et al.*, 2017). This lower-level RST system is mostly accompanied by upper-level zonal flow which implies an absence of disturbances that may induce rain formation or anti-cyclonic flow (e.g., Tsvieli and Zangvil, 2005; Lionello, 2012).

First attempts to identify the RST were made by Koplowitz (1973), Ben-Rubi (1980) and Ronberg (1984), as part of an automated classification of the regional synoptic systems. They based their methods on observations of Middle East meteorological stations and surface synoptic maps. Shafir *et al.* (1994) were the first to use gridded data for classification of EM synoptic systems.

The most widely used synoptic classification for the Levant is the semi-objective method of Alpert *et al.* (2004a, AOZS hereafter) which aimed to explain the weather conditions in Israel. This classification is applied to gridded data of the Levant, including the 1,000-hPa geopotential height, temperature, and wind components for 1200 UTC, obtained from National Center for Environmental Prediction/National Center for Atmospheric Research (NCEP/NCAR) reanalysis, at a $2.5^\circ \times 2.5^\circ$ resolution (Kalnay *et al.*, 1996; Kistler *et al.*, 2001) for the 27.5°–37.5°N, 30°–40°E domain. This classification started from five predefined groups of synoptic systems, which prevail over the Levant, namely Cyprus and Sharav Lows, Persian Trough, high pressure systems (Highs) and the RST. Each group of systems was further subdivided into a total of 19 synoptic types according to the features that are most relevant to the weather in Israel, such as the location and/or intensity of each type. The RST was divided into three types, depending on the relative geographical position of the trough axis with respect to longitude 35°E (the eastern coastline of the Mediterranean, exemplified in Figure 1a-c). Each type implies different weather conditions, which depend on the wind direction that is determined by the position of the axis (Ashbel, 1938; Saaroni *et al.*, 1998, 2010a). When the RST axis is to the west of longitude 35°E, the Levant is subjected to southeasterly winds, which advect hot and dry arid air masses into the region (see Figure 1a). In contrast, when the axis is east of this longitude, the winds blow from north and, together with the regional sea breeze, produced cool and moist advection from the Mediterranean Sea (see Figure 1c).

Tsvieli and Zangvil (2005) developed an automated algorithm for identifying the RST. However, this algorithm, based on sea-level pressure (SLP) alone, has been tailored to a specific Mediterranean subset of NASA, GEOS-1, developed by daSilva and Alpert (1996) and was applied for the domain 30°–34°N, 32.5°–40°E, for a short period of 11 years, 1985–1995. Krichak *et al.* (2012) developed an algorithm for identifying "active RST" events, which resembles the characteristics of "tropical-like storm" (Ziv *et al.*, 2005). The first step of Krichak *et al.* (2012) was to identify the RST through "a northward-oriented 1000-hPa trough extends from northeastern Africa to the EM within a target area of 22.5°–32.5°N, 25°–45°E." They started their search from 22.5°N in order to identify moisture transport from south. Awad and Almazroui (2016) developed an objective method for identifying the RST during the mid-winter (DJF), using SLP data from NCEP/NCAR reanalysis. They detected the location of the "main cyclone," over the 5°–22°N, 22.5°–45°E domain and the main trough that extends northward. They searched for the linkage between the RST and the major anti-cyclonic systems governing the Middle East, and found that the RST is oriented to the west when the Siberian High strengthens and to the east, when the Azores High is stronger. Awad and Mashat (2019) also showed that in the autumn season "the RST is oriented from the west to the east when the

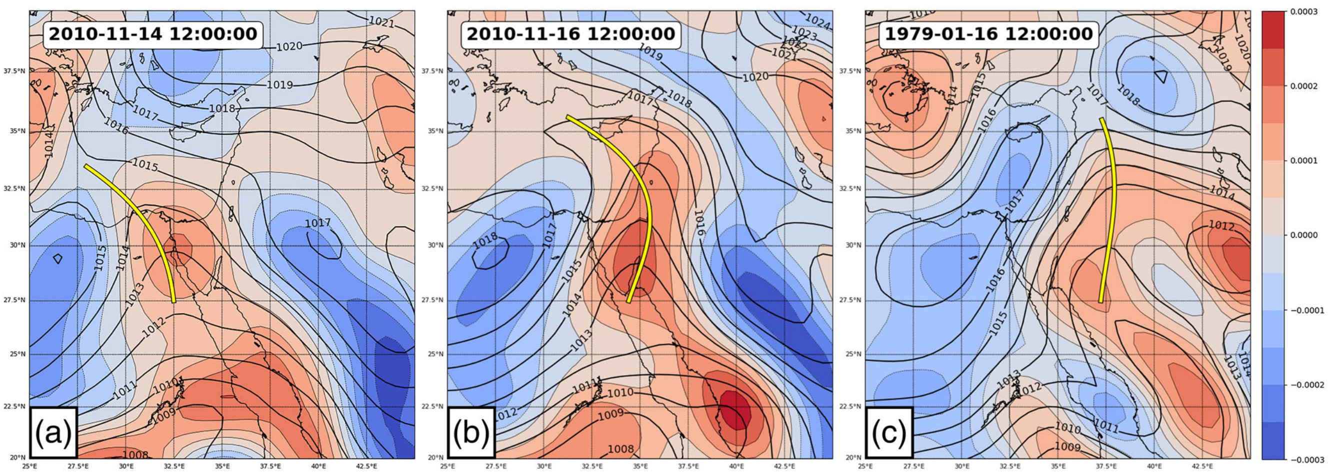


**FIGURE 1** SLP (hPa, black lines) and geostrophic vorticity ($s^{-1}$, colours), exemplifying the three types of RST according to its axis location: (a) to the west, (b) centre and (c) east of Israel. The axis in each figure, derived by the new algorithm (see Section 2), is represented by a thick yellow line [Colour figure can be viewed at wileyonlinelibrary.com]

Azores high extends eastward and the Siberian high shrinks eastward or shifts northward."

Dayan *et al.* (2012) evaluated the performance of the AOZS classification against subjective classification of their own, based on SLP maps, for a 10-year period (1995–2004). The highest agreement they found (>50%) was for synoptic systems characterized by sharp horizontal pressure gradients, such as Cyprus lows. However, for other systems, including the RST, the agreement was lower. Nevertheless, the AOZS classification is most widely used for climatological and applicative studies (e.g., Saaroni *et al.*, 2010b; Hochman *et al.*, 2018a, 2018b) since it covers the entire spectrum of the prevailing synoptic systems of the Levant.

The limitations of the previous methods described above, raise the need to develop an alternative method for an automatic identification and classification of the RST (both active and non-active). The proposed method focuses on the Levant as the "region of interest" (29°–33.5°N, 32°–38°E, see Figure 2, dashed rectangle) and intend to cope with curved or kinked axes, rather than only with straight meridional oriented axes.

Section 2 describes the algorithm developed and stresses the rationale behind its design. Section 3 evaluates the algorithm performance, elaborates its response to variations in the data sources and resolutions and presents climatological features of the RST. Section 4 discusses and summarizes the characteristics of our proposed new algorithm.

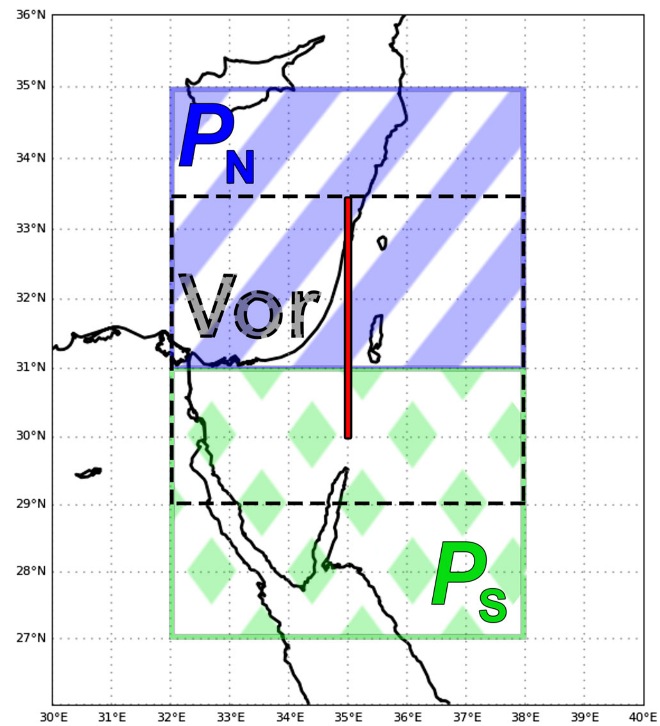


**FIGURE 2** The reference regions used for analysing the RST. The areas denoted $P_N$ (upper, purple rectangle) and $P_S$ (lower, green rectangle) are the northern and southern regions, respectively, over which the average SLP is calculated to verify pressure drop from north to south. The area denoted Vor (dashed rectangle) is the "region of interest," over which the vorticity is averaged. The thick (red) line along the 35°E longitude is used for determining where the RST axis is located relative to Israel [Colour figure can be viewed at wileyonlinelibrary.com]

## 2 | DATA AND METHODS

The purpose of the algorithm is to identify and classify RSTs, based on atmospheric data supplied by any data source, reanalysis or model outputs, regardless its spatial resolution. To achieve this goal, and to circumvent the weaknesses of previous classifications used in this region (described in Section 1), the domain used in this study is the Levant. The term RST used here follows the definition of Alpert *et al.* (2004a) and Tsvieli and Zangvil (2005), that is, a trough extending from the Red Sea northward. The fields used are the SLP and the relative geostrophic vorticity, which is derived from the SLP. The following steps were executed: pre-processing the input data, examining necessary conditions for RST existence, locating the trough axis and, if identified, classifying the RST to one of the three types.

## 2.1 | Input and pre-processing

To permit input data from different sources with various resolutions, data was first interpolated (spline interpolation) to a common grid, of 0.5° × 0.5° resolution. Following Pinto *et al*. (2005), the spline interpolation does not add any feature to the map, so it does not introduce artefacts to the data, such as meso-cyclones, but enables locating the RST axis more accurately. The same interpolation procedure was applied to the geostrophic vorticity field, which was calculated first from the raw data.

## 2.2 | Conditions for RST existence over the Levant

The study region is the Levant, defined as the "region of interest" (29°–33.5°N, 32°–38°E, see Figure 2, dashed rectangle). In order to ensure that the RST fulfils its basic features and that it dominates the region of interest, four conditions were imposed. Four trained weather forecasters (the authors of this article) defined these conditions, through trial and error experiments, after maximum agreement between automatically and subjectively identification of RST was achieved (see Section 3.1).

### 2.2.1 | SLP gradient condition

The first condition is the "SLP gradient," that is, that the SLP around the Levant decreases from north to south. The algorithm calculates the average SLP within two reference regions, extending north and south of the region of interest, that is, 31°–35°N, 32°–38°E and 27°–31°N, 32°–38°E (see upper and lower boxes, respectively, in Figure 2). Only if the average SLP over the northern box ($P_N$) is higher than that of the southern one ($P_S$), the SLP gradient condition is met.

### 2.2.2 | Vorticity condition

The second is the "vorticity condition." If the average geostrophic vorticity over the region of interest (defined above) is positive, the vorticity condition is met.

### 2.2.3 | No distinct closed cyclone condition

The third condition demands that no distinct closed cyclone, either a Sharav (North African) low or a winter low is located in the southern or eastern Levant and dominates the region of interest. This does not refer to meso-scale lows that may also develop within the RST-dominated area, but rather to synoptic-scale lows that often characterize the region. To capture well-defined lows, we searched for Sharav lows, at the 25°–32.5°N, 25°–35°E domain and for winter lows, at the 35°–42.5°N, 30°–35°E domain, the preferred domains for their development. Note that these reference regions extend beyond the region of interest, but are needed for the identification process. A low centre (SLP minimum) found in any of these domains was considered as dominating the region if it had a mean depth of at least 1.6 hPa at a radius of 300 km and of at least 0.75 hPa to each direction (to ensure sufficient symmetry of the pressure gradient around the pressure minimum). The threshold values were chosen and tuned through trial and error experiments. Figure 3 presents a case where a Sharav low over Egypt that dominated the region of interest could cause a false RST detection. The implementation of this condition avoided this misidentification. Note that the cyclone

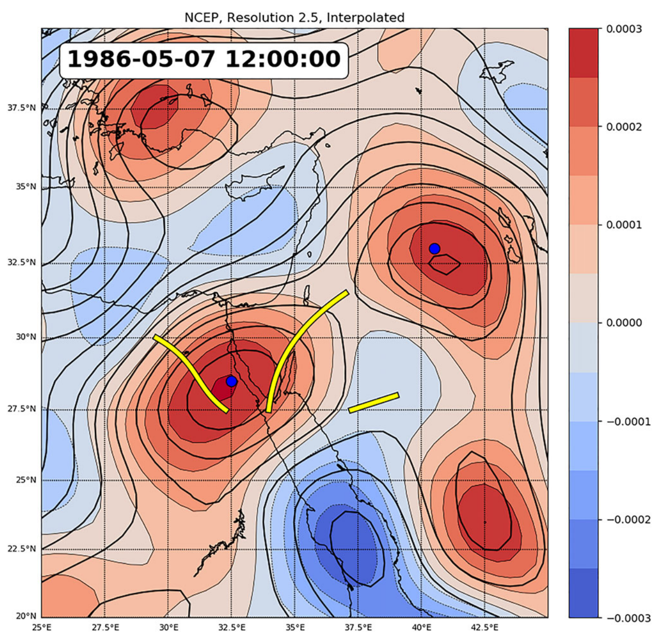


**FIGURE 3** As in Figure 1, but for May 7, 1986 1200 UTC, showing a case in which the first two conditions for an RST identification are met, but the third condition, concerning an existence of a nearby major cyclone indicates an incidental passage of a Sharav low. Therefore, this case is classified as "No RST." Note that the cyclones seen east of 40°E did not caused misidentification in this case [Colour figure can be viewed at wileyonlinelibrary.com]

seen east of 40°E did not cause misidentification in this case.

#### 2.2.4 | Existence of a distinct trough axis within the domain

The last condition for an RST identification is the existence of at least one candidate trough axis within the region of interest. If the trough axis did not exist or did not cross this region, the case was classified as "No RST." The procedure of identifying and typifying the RST axis is specified in Section 2.3.

### 2.3 | Locating the trough axis

The search for the trough axis starts from a reference region extending south, southeast and southwest of the region of interest (27.5°–30.5°N, 30°–42.5°E), to capture trough axes that originate from these directions, and to cope with curved or kinked troughs. The algorithm seeks for local SLP minima, which can be regarded as potential core of an RST axis that extends northward. A grid point was considered as belonging to a trough axis if it had the lowest SLP with respect to its neighbouring grid points along at least one of the four directions: north–south, east–west, northeast–southwest or northwest–southeast, at a distance of ~1.5°. This distance was chosen through trial and error experiments.

If a local minimum was found, the algorithm searched for another local minimum in its immediate neighbourhood (which is not to the south of it) that is a candidate for being the next point in the trough axis. As long as such minima were found, the algorithm kept searching further for possible next points in the trough. When none was found, the search stopped and the line connecting the aforementioned grid points was considered as the trough axis.

For many troughs, it was found that several trough axes merged into one, as is exemplified in Figure 4a. These were considered as one axis, and its path was considered as follows: for each latitude, in which at least one merging axis existed, the average longitude between the easternmost and westernmost of all merging axes was considered as the merged axis longitude for the pertinent latitude. This way, the algorithm eliminates multiple merging axes and leaves, at most, up to three axes at a map. Inspection of hundreds of cases (maps) indicated that very often, only one axis was identified. These merged axes were the candidates in the next step, when selecting the major RST axis for a given map (shown in Figure 4b). Due to the discrete process of its derivation, the trough axes look as a kinked chain of straight segments (Figure 4b), which therefore were smoothed, as is exemplified in Figure 4c.

Note that the after locating the trough axis, the case will be defined as an RST event only if the axis extends north of 30°N.

### 2.4 | RST classification

When all four conditions were met and the case was therefore defined as an RST, all merged troughs found were examined in order to select the dominant one, according which the RST would be classified. If more than one of the merged axes existed in a given map (see

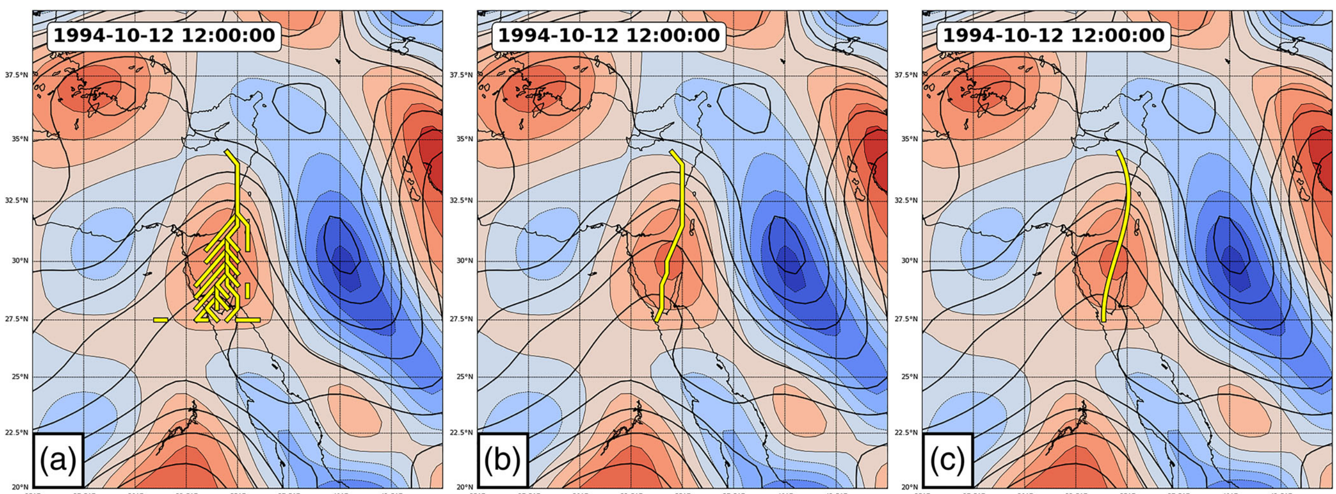


**FIGURE 4** As in Figure 1, but for October 12, 1994 1200 UTC, including all axes (a), the merged axis (b) and the smoothed merged axis (c) [Colour figure can be viewed at wileyonlinelibrary.com]

example in Figure 5), all merged axes received a geostrpohic voritcity (GV) score and the one with the highest score was selected as the RST axis for the pertinent map. A GV score is the sum of GV values at the grid points belonging to the axis ("line integral of the vorticity"). This selection method was found to effectively balance between the axis length and intensity, as both are important factors for selecting the right RST axis.

Each RST was then classified according to the relative location of its axis to the 35°E longitude (see thick red line in Figure 2). If the trough axis was found only to the East (West) of this longitude, it was classified as a trough with an eastern (western) axis. A trough with an axis that crosses the 35°E longitude was classified as an RST with a central axis. The RST shown in Figure 5 is an RST with an eastern axis.

## 2.5 | Data used

The algorithm was applied to various databases as follows: the ERA-Interim reanalysis (Uppala *et al.*, 2005; European Centre for Medium-Range Weather Forecasts, 2009; Dee *et al.*, 2011) with $0.75° \times 0.75°$ and $2.5° \times 2.5°$ spatial resolutions, along with the NCEP/NCAR reanalysis at a $2.5° \times 2.5°$ spatial resolution (Kalnay *et al.*, 1996; Kistler *et al.*, 2001). It should be noted that according to ERA documentation: "…data is on the fly transformed to a regular lat/lon grid, interpolated to your selected resolution …" (https://confluence.ecmwf.int/pages/viewpage.action?pageId=56658069) and the base resolution is of about 80 km (0.75°), smoothed by the European Centre for Medium-Range Weather Forecasts (ECMWF) to $2.5° \times 2.5°$. The comparison between the databases was based on the 1979–2016 period, corresponding to the availability of the ERA-Interim data.

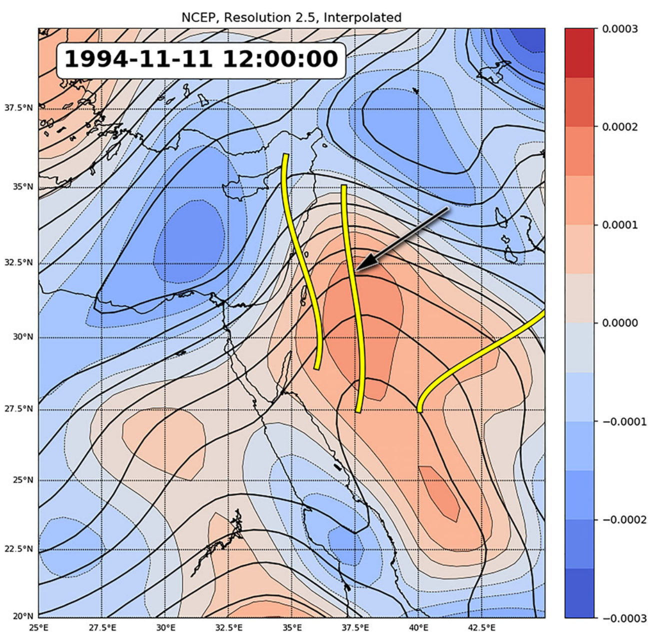


**FIGURE 5** As in Figure 1, but for November 11, 1994 1200 UTC, including three merged axes. The axis with the highest GV score (the central one, denoted by an arrow), was selected and therefore this RST was identified as "RST east" [Colour figure can be viewed at wileyonlinelibrary.com]

# 3 | RESULTS

## 3.1 | Evaluation of the algorithm

The skill of the new algorithm was evaluated by comparing it with a subjective identification and classification of the four trained weather forecasters. The subjective decision was based on the SLP and sea-level relative vorticity maps, derived from the NCEP/NCAR reanalysis database. The validation process was done in four stages. In each stage we compared the percentage of agreement between the algorithm identification and the subjective one for an individual sub-sample of randomly selected maps. The first stage included 200 maps identified by the algorithm as RST. Second, included 150 maps identified by the algorithm as "No RST." The remaining two stages were based on subjective identification, so that in Stage #3, 100 maps subjectively identified as RST were compared with the algorithm identification, and in Stage #4, this was done for 150 maps subjectively identified as "No RST." Table 1 presents the percentage of agreement found between the algorithm and the subjective identification for the four validation experiments (stages), total of 600 maps. The chosen days were not taken from the months July–August, in which RST does not prevail (see Section 1 and the climatological results in Section 3.4).

The degree of agreement between the automated identification and the subjective one is high, and varies between 87 and 96% (see Table 1). The subset of maps identified by both the algorithm and the weather forecasters as RST were further compared for the classification of the specific type, that is, whether it is an RST to the "east," "west" or "central." Here, the agreement on the specific type was 79%. These results imply that the algorithm is acceptable for climatological research as well as for operational use. Frakes and Yarnal (1997) succeeded to replicate 90% of the synoptic systems over Europe during the winter season "when pressure patterns are usually well defined with steep gradients" and only 60% in the summer, when the systems are weaker. The typical pressure variability of the RST is in the order of that typifying summer European systems, that is, ~10 hPa (see e.g., Figure 1). Therefore, the 79%

**TABLE 1** Percentage of agreement between the automatic algorithm and the subjective RST identification, done on maps based on NCEP/NCAR reanalysis database for 1200 UTC, for the period 1979–2016

| | Stage | No. of scanned maps | Agreement between algorithm and subjective identification (%) | Agreement between algorithm and subjective identification (%) |
|---|---|---|---|---|
| Algorithm identification | 1. Algorithm identified RST | 200 | 96 | |
| | 2. Algorithm identified no RST | 150 | 95 | |
| Subjective identification | 3. Subjective identified RST | 100 | | 87 |
| | 4. Subjective identified no RST | 150 | | 90 |
| Total | | 600 | | |

duplication rate achieved by our algorithm for the RST classification can be regarded as satisfactory.

In addition, the detection skill of the algorithm was estimated using several indices, based on the following measures: $h$, the number of "hits," that is, correct detection of RST, $f$, the number of "false" identification, in which the algorithm identified an RST but the subjective identification did not, and $m$, the number of "missed" identification, in which the algorithm failed to detect an RST that existed according to the subjective identification. The numerical values of $h$, $f$ and $m$ were 96, 4 and 5%, respectively. The percentage of "No RST" identifications that was found correct was 95% (Table 1). Three evaluation scores were applied; the positive predictions value (PPV, Equation (1)), the probability of detection (POD, Equation (2)), and the false alarm rate (FAR, Equation (3)):

$$\mathrm{PPV} = h/(h+f), \tag{1}$$

$$\mathrm{POD} = h/(h+m), \tag{2}$$

$$\mathrm{FAR} = f/(h+f). \tag{3}$$

Perfect detection skill is represented by PPV = 1.0, POD = 1.0 and FAR = 0.0. The respective scores for the algorithm, being 0.96, 0.95 and 0.04, are rather close to "perfect detection."

## 3.2 | Comparison with the AOZS classification

The skill of our algorithm in identifying RST was also compared with that of the previously used AOZS method (Alpert *et al.*, 2004a). As a first step, the AOZS identification of RSTs was evaluated against a subjective identification (as done for our algorithm, see Section 3.1). In the second step, the current algorithm and the AOZS identification method were compared.

The comparison between the AOZS and the subjective identification showed 76% agreement (regardless of the axis location), which is lower than the 87–96% obtained for the current algorithm (Table 1). The agreement between the current algorithm and the AOZS identification was only 61%. The relatively low performance of the AOZS identification of RSTs is consistent with the evaluation done by Dayan *et al.* (2012, see Section 1). This comparison exposed the difficulty of the AOZS method to distinguish between the RST and other synoptic systems that tend to appear simultaneously with the RST. Such are: high located to the north, west or east of Israel or a weak Cyprus low located north of Cyprus (see, e.g., Saaroni *et al.*, 1998 and Figures 6 and 7).

Figure 6 demonstrates the identification difficulties associated with the co-existence of an RST and other synoptic types, especially high-pressure systems. The blue (brown) bars show the distribution of days identified by the current algorithm as RST east (central) among the various synoptic types according the AOZS classification. The three bars to the left reflect the agreement among the two classification methods on the RST itself, 64% agreement on RST with an eastern axis and 58% on RST with a central axis. The others, spread over 10 synoptic types, reflect situations in which the AOZS classification defined the day as dominated by other synoptic type, while the current algorithm identified it as an RST. The most frequent disagreements are with "high to the west," "high to the east" and "high to the north" types. Examples of maps, which the current algorithm identified as RST and the AOZS identified as belonging to "high to the west," "high to the east" and "high to the north," are shown in Figure 7a–c, respectively.

Figure 7a shows a ridge that extends from the west, along the north African coast, towards the Sinai Peninsula, co-existing with an RST east of the Levant. The "decision" of the current algorithm to classify this map as an RST stems, on top of the RST intrusion from south, from the average positive vorticity over the region of interest (small solid rectangle), a factor not included in the AOZS method. Note that the AOZS method, that is based on a larger domain (the large dashed rectangle), classified this case as "high to the west." Figure 7b shows a case, defined by the AOZS as "high to the east," due to a ridge extending east of the region of interest, but not over the Levant, which was dominated by an RST with average positive vorticity. Figure 7c shows a case in which the majority of the EM was influenced by the southern margins of a large high pressure system from north, which caused the AOZS to classify it as "high to the north." Here also the Levant was dominated by an RST with dominating positive vorticity. These three examples demonstrate how relatively large synoptic systems may obscure smaller-scale systems, such as the RST, which is more relevant to the weather conditions in the region of interest, on which the current algorithm concentrates.

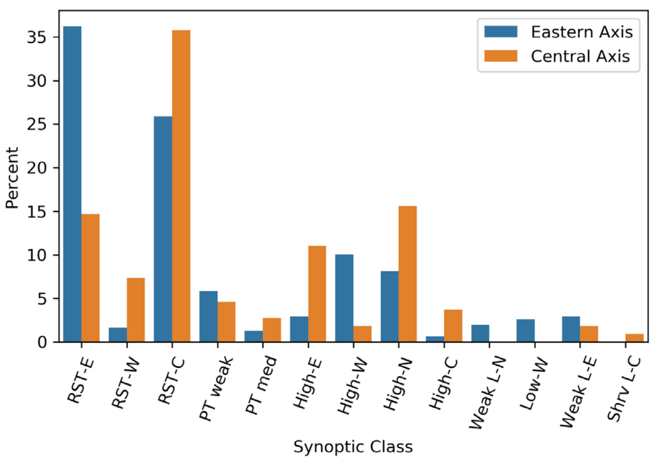


**FIGURE 6** Distribution of sample of days (randomly selected) categorized by the algorithm as RST with eastern axis (blue) and central axis (brown) as defined by the AOZS classification (of Alpert *et al.*, 2004a), which distinguish among 19 types [Colour figure can be viewed at wileyonlinelibrary.com]

The difficulty of the AOZS method in identifying correctly the RST may stem from several factors. The major is the approach underlying their method, which is designed to cover all regional synoptic system, rather than just the RST. This led them to use a larger region of interest (27.5°–37.5°N, 30°–40°E), within which each of the 25 grid points has a similar weight in the calculations. Furthermore, the AOZS method does not include any quantitative criterion that determines whether a cyclonic or an anti-cyclonic system dominates.

The current algorithm overcomes the above difficulties by choosing a much smaller region of interest, 27% of that used by the AOZS method, and by adopting a quantitative criterion that differentiates between dominant cyclonic or anti-cyclonic system, that is, the average relative vorticity over the region of interest.

## 3.3 | Distribution of RST as a function of database and horizontal resolution

Identification and classification of the RST, when applied to different databases, can expose differences among them, which may result from differences in the analysis methods and spatial resolutions. Here we compare the

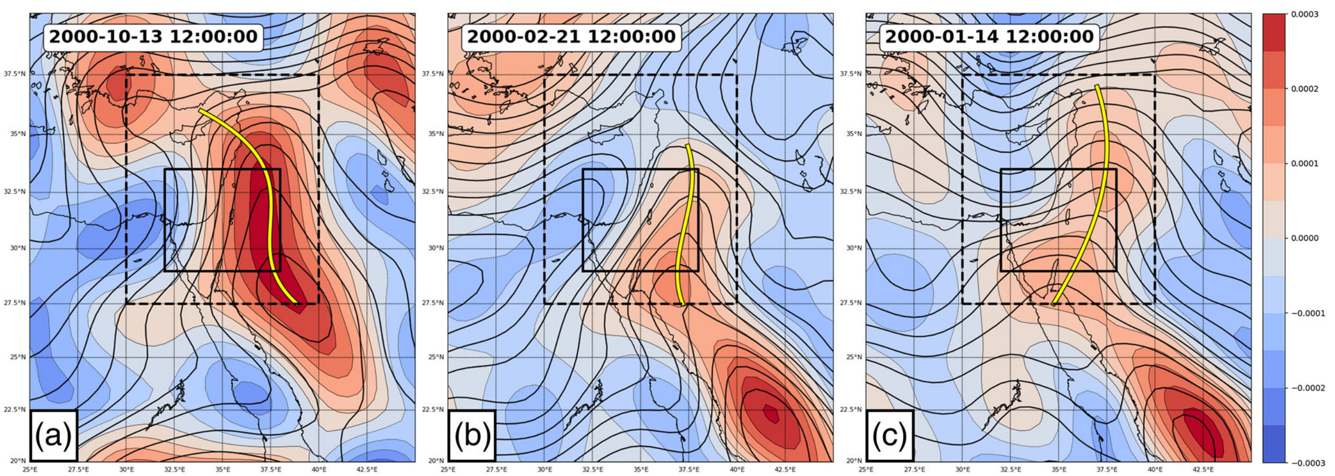


**FIGURE 7** As in Figure 1, for three cases (the dates are denoted in the figures) in which the algorithm identified as RST and the AOZS method classified as "high to the west" (a), "high to the east" (b) and "high to the north" (c). The large rectangle (dashed rectangle) in each map is the domain used by the AOZS method and the small rectangle (continuous line) denotes the region of interest of the present algorithms [Colour figure can be viewed at wileyonlinelibrary.com]

three databases, specified in Section 2.5. The first difference appears in the frequencies of RST days. The percentage increases from 17.6% for the ERA-Interim with $0.75^\circ \times 0.75^\circ$ resolution, to 20.6% for the ERA-Interim with $2.5^\circ \times 2.5^\circ$ resolution to 24.6% for the NCEP/NCAR reanalysis ($2.5^\circ \times 2.5^\circ$ resolution).

Table 2 specifies the RST frequencies according to the three databases. This enables a comparison between the two data centres (ERA-Interim and NCEP/NCAR), when based on the same resolution ($2.5^\circ \times 2.5^\circ$) on the one hand, and to assess the effect the spatial resolution has on the identification and classification from the same source (ERA-Interim), on the other hand. The lower frequency, found for the data with the finer resolution, may stem from the tendency of the high-resolution data to reflect sub-synoptic features, for example, meso-scale cyclones (as discussed by Ziv *et al*., 2015). These features disrupt the continuity of trough lines and, therefore, reduce the number of identified RSTs. It should be noted that the ERA-Interim data with the $2.5^\circ \times 2.5^\circ$ resolution is just a smoothed version of the original dataset, of $0.75^\circ \times 0.75^\circ$ resolution. The smoothing procedure eliminates small-scale features and thus improves the identification skill of the RST.

The numbers along the diagonal of Table 2 (bold) denote the identical identifications and classification between the pertinent two datasets, for each category, that is, “No RST,” “RST east,” “RST central” and “RST west,” If two datasets classify the RST similarly, the respective matrix would be diagonal. The percentage of perfect match is the percentage of days in which the identification and classification according to the two datasets compared is identical. These cases appear in the diagonal of the matrix (bold in Table 2). The percentage of mismatch refers to the cases in which according to one data source the case is defined as an RST and according to the other as “No RST.”

The highest perfect match, of similar identification and classification, was found between the two datasets of the ERA-Interim, being 87%. The mismatch of the RST identification between them was the lowest, only 8%, that is, in 92% of the cases both datasets identified RSTs. This high agreement stems, presumably, from the fact that the ERA-Interim data with spatial resolutions of $2.5^\circ \times 2.5^\circ$

**TABLE 2** Comparison of RST identification and classification among NCEP/NCAR reanalysis with $2.5^\circ \times 2.5^\circ$ resolution, ERA-Interim with $2.5^\circ \times 2.5^\circ$ resolution and ERA-Interim with $0.75^\circ \times 0.75^\circ$ resolution

| | | **ERA 0.75° × 0.75°** | | | |
|---|---|---|---|---|---|
| | | **No RST** | **East** | **Central** | **West** |
| **NCEP (2.5° × 2.5°)** | **No RST** | **9,916** | 251 | 206 | 90 |
| | **East** | 1,222 | **592** | 630 | 78 |
| | **Central** | 195 | 65 | **404** | 61 |
| | **West** | 100 | 22 | 34 | **14** |
| Agreement: Perfect match **79%** and misidentification **15%** | | | | | |
| | | **ERA 2.5° × 2.5°** | | | |
| | | **No RST** | **East** | **Central** | **West** |
| **NCEP (2.5° × 2.5°)** | **No RST** | **9,926** | 283 | 156 | 98 |
| | **East** | 870 | **785** | 729 | 138 |
| | **Central** | 143 | 55 | **364** | 163 |
| | **West** | 80 | 27 | 38 | **25** |
| Agreement: Perfect match **80%** and misidentification **12%** | | | | | |
| | | **ERA 2.5° × 2.5°** | | | |
| | | **No RST** | **East** | **Central** | **West** |
| **ERA (07.5° × 0.75 )** | **No RST** | **10,658** | 419 | 240 | 116 |
| | **East** | 163 | **521** | 199 | 47 |
| | **Central** | 143 | 171 | **773** | 187 |
| | **West** | 55 | 39 | 75 | **74** |
| Agreement: Perfect match **87%** and misidentification **8%** | | | | | |

*Note:* The statistics is based on the 1200 UTC maps. The period is 1979–2016, total of 13,880 days. Pronounced disagreements are underlined.

is a smoothed version of the original dataset, of $0.75° \times 0.75°$ resolution. The lowest value of perfect match was found between the NCEP/NCAR ($2.5° \times 2.5°$ resolution) and the fine resolution ($0.75° \times 0.75°$) dataset of ERA-Interim, 79%. The percentage of mismatch of the RST identification between them was found to be the largest, 15%. This reflects the joint effect of both the different resolutions and different reanalysis methods.

Differences between the data sources can be further elaborated from the off-diagonal numbers, reflecting local biases. The largest off-diagonal number in Table 2 is 1,222 (in the uppermost block), which compares between the ERA-Interim data with a $0.75° \times 0.75°$ resolution and the NCEP/NCAR dataset with a $2.5° \times 2.5°$ resolution. It denotes that 8.8% of the maps that the ERA-Interim with $0.75° \times 0.75°$ resolution identified as "No RST," the NCEP/NCAR identified as "RST east." A similar trend, though slightly weaker (6.2% of the maps), was found between the two databases with the same ($2.5° \times 2.5°$) resolution. These biases reflect a tendency of the ERA-Interim to classify as "No RST" a part of the RSTs identified based on the NCEP/NCAR. It may result from two possible reasons, the first is that the trough axis is found east of the region of interest while using ERA-Interim data, and the second is that according to this database no distinct axis was identified. Examples of these two cases were found (not shown). Also, differences in the assimilation and analysis methods of each data centre may result in differences in the resulting SLP maps, especially in regions with low density of meteorological stations such as the Middle East.

## 3.4 | Climatological aspects of the RST

### 3.4.1 | Annual and inter-annual variations

Figure 8 shows the annual distribution of RSTs according the three databases. The annual frequency is 24.6% according NCEP/NCAR reanalysis and 20.6 and 17.6% according the ERA-Interim with $2.5° \times 2.5°$ and $0.75° \times 0.75°$ resolutions, respectively. This indicates a typical annual occurrence in the order of 20%, most similar to the 23% found by Alpert *et al.* (2004a) and the 19% found by Tsvieli and Zangvil (2005). A similar seasonal dependence is well noticed among the three databases, with the following common characteristics; the autumn is the main RST season, with a maximum in November and a gradual and consistent decrease from December towards the yearly minimum, in July. This course is consistent with that shown by Alpert *et al.* (2004b). It should be noted that Tsvieli and Zangvil (2005) found the main autumn peak in October and a secondary peak in April (see fig. 3 and Table 1 in their paper). Awad and Mashat (2019) found that RST extending north of 20°N persists during 50% of the autumn season, and Awad and Almazroui (2016) found 38% occurrence of RST for the winter season. The considerably higher occurrence shown in the latter two studies may be explained by the larger study area they used compared to that used in the present study.

The degree of similarity in the inter-annual and the inter-monthly variations in RST occurrence among the various data sources and resolutions was analysed through correlating the RST occurrence among the three datasets. When correlating inter-annual variations (38 points, i.e., years, in time), the correlation between the NCEP/NCAR reanalysis and the ERA-Interim (both with $2.5° \times 2.5°$ resolution) was 0.92. The same correlation was found between the $0.75° \times 0.75°$ and the $2.5° \times 2.5°$ data resolutions of the ERA-Interim. When the monthly data were correlated (456 points, i.e., months, in time) the correlations dropped to 0.70 and 0.63, respectively. All the correlations are significant at the 0.01 level. The similarity in the annual course and the high correlations in the inter-annual and inter-monthly variations among the various datasets indicate that the detailed structure of various databases preserve the temporal variability of the RST frequency of occurrence.

Another feature analysed was the distribution of RST events, that is, sequences of RST days. Figure 9 presents the distribution of the duration of RST events (according to the NCEP/NCAR reanalysis database). The most frequent duration is 1 day, but 46% of the RST days are

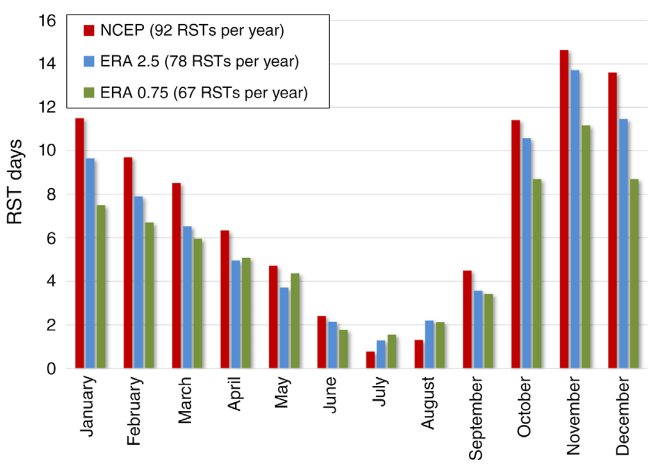


**FIGURE 8** Annual monthly variations of RST days according to the NCEP reanalysis data (red), and ERA-Interim with $2.5° \times 2.5°$ and $0.75° \times 0.75°$ resolutions (blue and green, respectively), for the period 1979–2016 [Colour figure can be viewed at wileyonlinelibrary.com]

included within long events, of ≥4 days duration, and that over half of the events last 2 days and more, up to a sequence of 17 days. These findings reflect the quasi-stationary character of this synoptic system, in agreement with Saaroni *et al*. (1998) and Ziv *et al*. (2005).

### 3.4.2 | Diurnal variation

One assumption of this study is that the northward part of the RST, over the Levant, is expected to respond to diurnal variations in the temperature contrast between the Mediterranean Sea and the adjacent land to the east. Therefore, the RST is expected to move eastward, inland, during the day hours and westward, towards the sea, during the night hours.

Figure 10 shows two composite maps of the days in which RST was identified (based on the NCEP/NCAR reanalysis). One is for 0000 UTC (Figure 10a), which represent the night hours in the Levant (0200 LST) and the other for 1200 UTC (Figure 10b), representing the noon hours (1400 LST). It is clearly seen that in the day hours there is an eastward shift of the axis, ~5° longitudes, with respect to its position in the night hours. In the day hours it extends along 39°–40°E, over the warmer land, and in the night hours, around 34°E, over the sea, which then becomes warmer than the adjacent land. Similar results were found when applying the algorithm on the ERA-

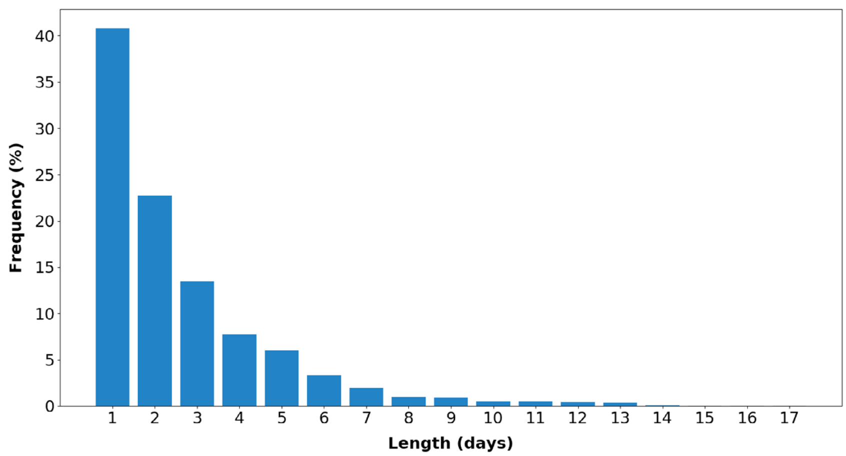


**FIGURE 9** Distribution of the duration of RST events according to the NCEP reanalysis data (1979–2016) [Colour figure can be viewed at wileyonlinelibrary.com]

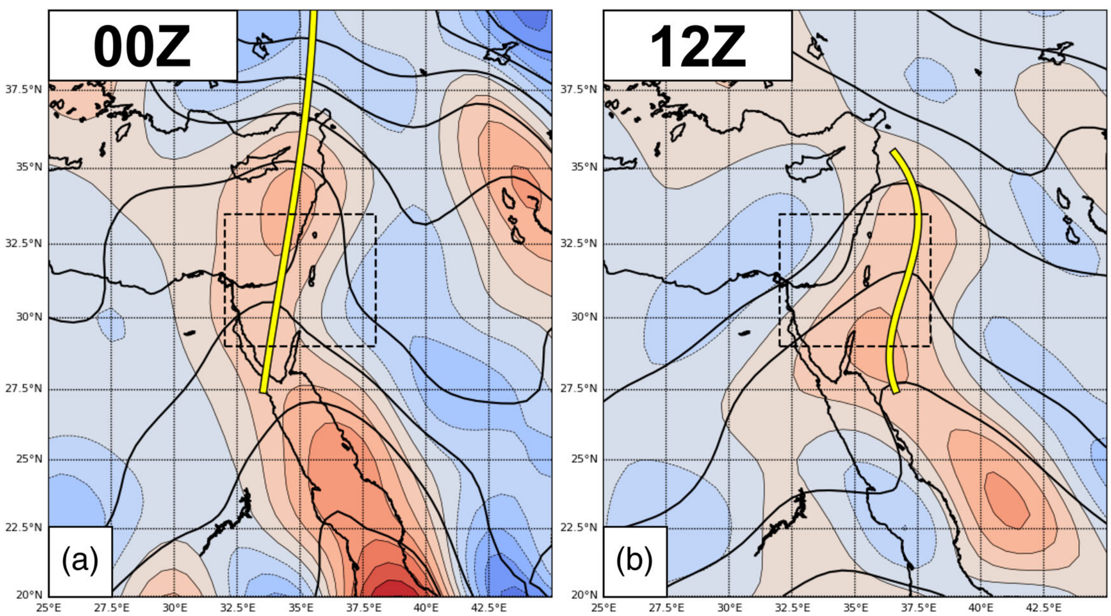


**FIGURE 10** As in Figure 1, but composite maps for all days in which RST was identified based on the NCEP reanalysis for (a) 0000 UTC and (b) 1200 UTC (1979–2016). The RST axis is derived as is done for the individual maps (see Section 2.3). The region of interest used for identifying the RST is shown by dashed rectangle [Colour figure can be viewed at wileyonlinelibrary.com]

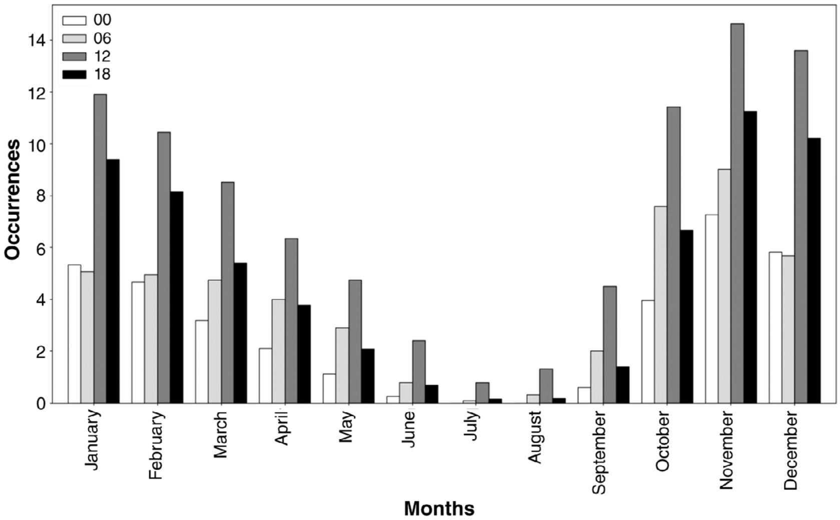


**FIGURE 11** Annual variations of RST occurrences (average number per month) at 0000 UTC (white), 0600 UTC (light grey), 1200 UTC (dark grey) and 1800 UTC (black), according to the NCEP reanalysis data (1979–2016)

Interim database, though with a smaller shift (not shown). It is worth noting that a tendency of cyclones to move towards the sea and to strengthen during the night was first shown by Alpert *et al*. (1990) for Mediterranean cyclones.

Figure 11 shows annual variations of RST occurrences at the 0000, 0600, 1200 and 1800 UTC. It further indicates the higher occurrence of RST during noontime, being almost twice than the occurrence at 0000 and 0600 UTC. Second is the occurrence at 1800 UTC, being ~20% lower than at 1200 UTC. Similar tendencies were shown by Tsvieli and Zangvil, 2005 (see fig. 5 in their article), though with much smaller magnitudes.

### 3.4.3 | Long-term trends

Alpert *et al*. (2004a), based on the NCEP/NCAR reanalysis, found a pronounced increase in RST occurrence between the years 1948 and 2000. The increase was mostly from the 1960s, a decade they showed to have the lowest occurrence. In order to assess the persistence of this trend, and to associate it with the global warming period since the late seventies, we present the interannual variation and the long-term trend of RST occurrence for 1979–2016, based on the three datasets. This was done separately for the entire year (Figure 12a–c) and for the peak months of RST occurrence, October–December (Figure 12d–f).

The analysis for the entire year, based on the NCEP/NCAR reanalysis data (Figure 12a), shows a decreasing trend, of 4.7 days per decade, significant at the .01 level. For the ERA-Interim with $2.5° \times 2.5°$ resolution (Figure 12b), a decreasing trend is also noted, but statistically insignificant. In contrast with the above, a similar analysis based on the ERA-Interim with $0.75° \times 0.75°$ resolution (Figure 12c) shows an increasing trend, though very small and statistically insignificant. The same analysis, for the months October–December, which contain ~40% of the RST occurrences, yielded the same trends, but none of them was found statistically significant.

The mixed signs of the trends found, together with the fact that only one out of the six trends was found statistically significant, suggest that during the current period, characterized by a persistent global warming, no distinct trend in RST occurrence can be noted.

## 4 | SUMMARY AND DISCUSSION

This study presents a new algorithm, which automatically identifies the northern part of the RST, over the Levant, and classifies it according to the location of the trough axis with respect to longitude 35°E. This algorithm focuses on a specific system, over a limited area, as opposed to the common classification methods, which purpose was to identify and classify all synoptic systems in the Levant region (Alpert *et al*., 2004a; Dayan *et al*., 2012).

The algorithm utilizes the SLP and the sea-level relative geostrophic vorticity fields. These two fields are interpolated into a common grid, of $0.5° \times 0.5°$ resolution. The interpolated data undergo a series of examinations in order to verify whether an RST is identified. The basic conditions check whether the situation meets the RST definition, that is, a pressure drops from north to south, average positive relative vorticity exists over the defined region of interest and a distinct continuous trough axis extends from south into the region of interest. An additional condition was imposed to prevent false identifications in cases in which a pronounced closed cyclone

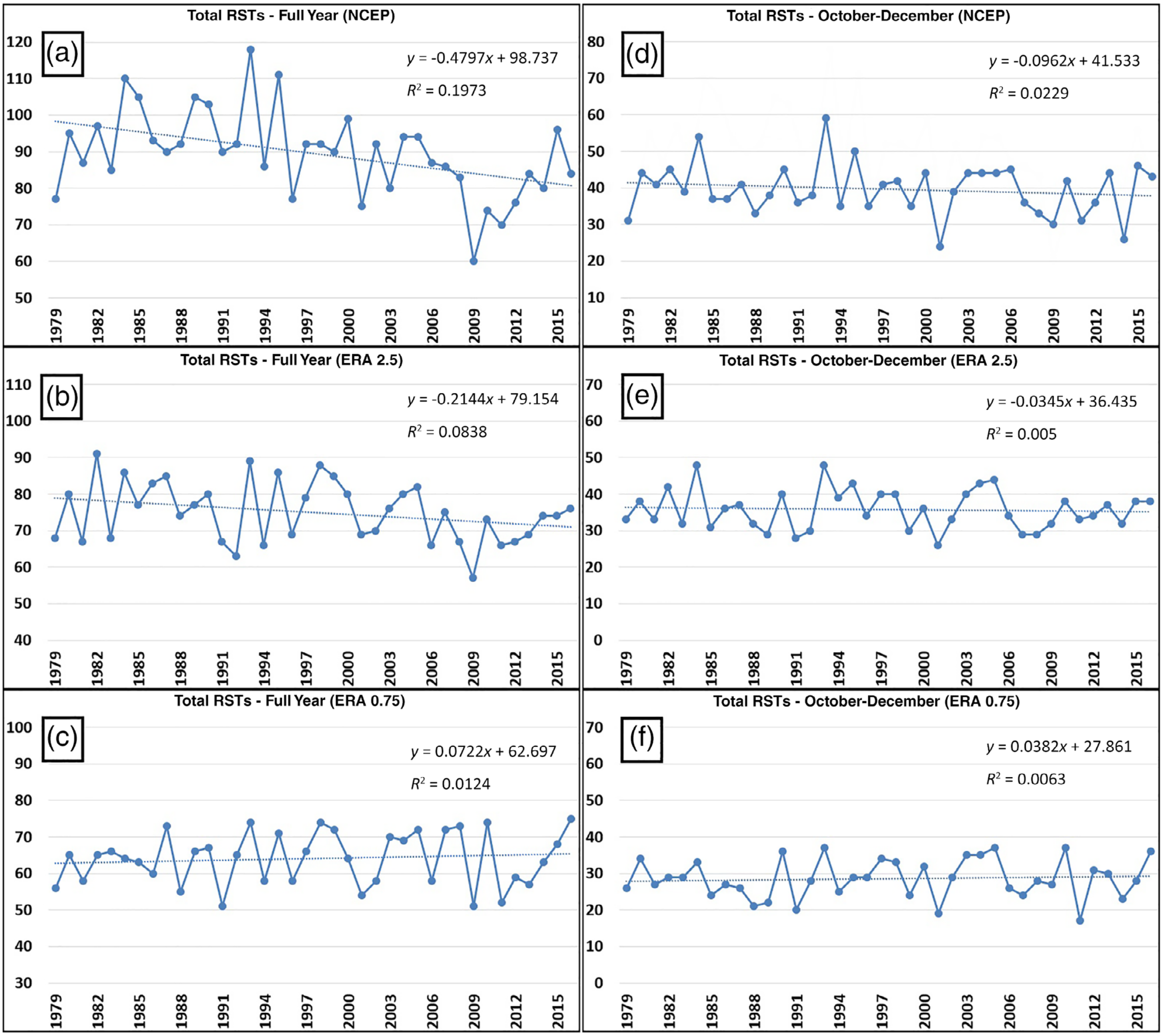


**FIGURE 12** Inter-diurnal variation in the occurrence of RST (no. of days per year, a–c) and for the peak season of RST, October–December (d–f). Based on the NCEP/NCAR reanalysis (2.5° × 2.5° resolution, a and d), the ERA-Interim (2.5° × 2.5° resolution, b and e) and the ERA-Interim (0.75° × 0.75° resolution, c and f), for the period 1979–2016. In each graph, the linear trend (dotted line) and $R^2$ are added [Colour figure can be viewed at wileyonlinelibrary.com]

(such as a Sharav low or a winter low) dominates the region of interest.

The classification of the RSTs according to the axis location, from the mathematical point of view, differentiates among two distinct pure types, the eastern and western axes, with respect to longitude 35°E. A third one, hybrid in nature, for which the axis extend partly to the east and partly to the west of that longitude, is defined as a central axis. This approach is in line with the definition of "RST with central axis" by Alpert *et al.* (2004a).

From the "weather point of view," the two pure types are associated with definite uniform weather conditions over the Levant. The third type implies different weather conditions over the different parts of the Levant. For instance, during two cases the axis crossed central Israel so in the northern part of Israel strong dry easterly winds produced severe forest fires (in the Carmel mountains near Haifa on the beginning of December 2010 and towards the end of November 2016, in the city of Haifa) and the southern Mediterranean coast of Israel was under northerly moist winds.

In order to examine the flexibility of the algorithm, which was developed for being applicable for a wide spectrum of data sources and resolutions, it was applied to NCEP/NCAR reanalysis, with a 2.5° × 2.5° resolution and to ERA-Interim with spatial resolutions of 0.75° × 0.75° and its smoothed version, of 2.5° × 2.5°. The use of fine resolution data exposed the effect of meso-scale features (noise), which reduced the number of identified RSTs by 15%. The evaluation of the algorithm's reliability was done by comparing its RST identification to that of trained weather forecasters, on 600 randomly selected maps. The three evaluation scores used, the PPV, the POD and the FAR were close to those defining perfect detection skills.

The new algorithm proposed here overcomes some of the major weaknesses of the commonly used synoptic classifications for the Levant. The main improvement stems from the focus, given to the RST alone. Second, is the choice of the region of interest, that is, the centre of the Levant, a region of $4.5^\circ \times 6^\circ$, that is, 1/4 of the area used by the AOZS. Third is the inclusion of the relative vorticity field as an indicator for the RST identification. Another advantage is that the algorithm is capable of tracking the trough axis even when it is not oriented in the south–north direction and even when it is curved or kinked.

The annual frequency of the RST varied between 17.6 and 24.6% among the three datasets used. This confirms that the RST is the second most frequent synoptic system in the region, after the Persian trough (Alpert *et al.*, 2004a, 2004b). The largest biases were found between the NCEP/NCAR (with $2.5^\circ \times 2.5^\circ$ resolution) and ERA-Interim (with $0.75^\circ \times 0.75^\circ$ resolution). These biases can be attributed to the fact that high horizontal resolution implies a tendency to resolve sub-synoptic features, which may disrupt the continuity of trough lines and therefore, to reduce the number of identified RSTs. Differences between the results based on the NCEP/NCAR and the ERA-Interim databases at a similar resolution ($2.5^\circ \times 2.5^\circ$) may be attributed to the fact that the ERA-Interim processing system works in higher horizontal and vertical resolutions and that it is a smoothed version of the $0.75^\circ \times 0.75^\circ$ resolution data. In addition, differences in the assimilation and analysis methods of each data centre may change the resulting SLP maps, especially in regions with low density of meteorological stations such as the Middle East.

In spite of the differences described above, the annual distribution of the RST is most similar according the three datasets, with the maximum from October until December, occupying 44.3, 45.9 and 42.6% of the annual RST days, according the NCEP/NCAR and the ERA-Interim with $2.5^\circ \times 2.5^\circ$ and $0.75^\circ \times 0.75^\circ$ resolution, respectively. The peak month is November, with a gradual and consistent decrease from December towards the yearly minimum in July.

The application of our algorithm on day and night maps separately, showed, for the first time, that the RST trough has a significant diurnal oscillation. It tends to be near the eastern coast of the Mediterranean at nighttime and to shift eastward (inland) at noontime, presumably due to the warming of the continent during the day hours. This indicates that the RST, though being a synoptic-scale system, has meso-scale features, at least in its northern end, at the Levant region.

The long-term variations in the occurrence of RST, analysed for the 1979–2016 period, shows mostly small, inconsistent and insignificant trends. It can be concluded that generally, no distinct long-term trend can be noted during the period of the persistent global warming.

An important missing link in the RST classification is the absence of any automatic method capable of distinguishing between "active RST," which is accompanied by tropical-like weather conditions, and "non-active" (dry) RST. The development of such an algorithm is the next step of the research.

## ACKNOWLEDGEMENTS

The authors thank the Israeli Science Foundation (ISF, grant number 1123/17).

## ORCID

*Hadas Saaroni* https://orcid.org/0000-0001-6369-1847

## REFERENCES

Alpert, P., Neeman, B.U. and Shay-El, Y. (1990) Climatological analysis of Mediterranean cyclones using ECMWF data. *Tellus*, 42A, 65–77.

Alpert, P., Osetinsky, I., Ziv, B. and Shafir, H. (2004a) Semi-objective classification for daily synoptic systems: application to the eastern Mediterranean climate change. *International Journal of Climatology*, 24, 1001–1011.

Alpert, P., Osetinsky, I., Ziv, B. and Shafir, H. (2004b) A new seasons definition based on the classified daily synoptic systems, an example for the eastern Mediterranean. *International Journal of Climatology*, 24, 1013–1021.

Alpert, P. and Ziv, B. (1989) The Sharav Cyclone: observations and some theoretical considerations. *Journal of Geophysical Research. Atmospheres*, 941(D15), 18495–18514.

Ashbel, D. (1938) Great floods in Sinai Peninsula, Palestine, Syria and the Syrian Desert, and the influence of the Red Sea on their formation. *Quarterly Journal of the Royal Meteorological Society*, 64, 635–639.

Awad, A.M. and Almazroui, M. (2016) Climatology of the winter Red Sea trough. *Atmospheric Research*, 182, 20–29.

Awad, A.M. and Mashat, A.W.S. (2019) Climatology of the autumn Red Sea trough. *Theoretical and Applied Climatology*, 135(3–4), 1545–1558.

Ben-Rubi, P. (1980) An objective definition of Red Sea trough in Israel. MSc Thesis, Jerusalem, The Hebrew University of Jerusalem (in Hebrew).

daSilva, A. and Alpert, P. (1996) Documentation of the multi-year GEOS-1 assimilation data subset for Northern Africa, the Mediterranean and the Middle East. DAO Office Note 96-05. NASA, Goddard Space Flight Center, 24 pp.

Dayan, U., Tubi, A. and Levy, I. (2012) On the importance of synoptic classification methods with respect to environmental phenomena. *International Journal of Climatology*, 32, 681–694.

Dayan, U., Ziv, B., Shoob, T. and Enzel, Y. (2008) Suspended dust over southeastern Mediterranean and its relation to atmospheric circulations. *International Journal of Climatology*, 28, 915–924.

Dee, D.P., Uppala, S.M., Simmons, A.J., Berrisford, P., Poli, P., Kobayashi, S., Andrae, U., Balmaseda, M.A., Balsamo, G., Bauer, P., Bechtold, P., Beljaars, A.C.M., van de Berg, L., Bidlot, J., Bormann, N., Delsol, C., Dragani, R., Fuentes, M., Geer, A.J., Haimberger, L., Healy, S.B., Hersbach, H., Hólm, E. V., Isaksen, L., Kållberg, P., Köhler, M., Matricardi, M., McNally, A.P., Monge-Sanz, B.M., Morcrette, J.J., Park, B.K., Peubey, C., de Rosnay, P., Tavolato, C., Thépaut, J.N. and Vitart, F. (2011) The ERA-Interim reanalysis: configuration and performance of the data assimilation system. *Quarterly Journal of the Royal Meteorological Society*, 137(656), 553–597.

El-Fandi, M.G. (1948) The effect of the Sudan monsoon low on the development of thundery conditions in Egypt, Palestine and Syria. *Quarterly Journal of the Royal Meteorological Society*, 74, 31–38.

El-Fandy, M.G. (1950) Effects of topography and other factors on the movement of lows in the Middle East and Sudan. *Bulletin of the American Meteorological Society*, 31(10), 375–381.

Enzel, Y., Amit, R., Dayan, U., Crouvi, O., Kahana, R., Ziv, B. and Sharon, D. (2008) The climatic and physiographic controls of the eastern Mediterranean over the late Pleistocene climates in the southern Levant and its neighboring deserts. *Global and Planetary Change*, 60, 165–192.

Erel, Y., Tirosh, O., Kessler, N., Dayan, U., Belkin, S., Stein, M., Sandler, A. and Schauer, J.J. (2013) Atmospheric particulate matter (PM) in the Middle East: toxicity, trans-boundary transport, and influence of synoptic conditions. In: Censi, P., Darrah, T. and Erel, Y. (Eds.) *Medical Geochemistry—Geological Materials and Health*. Dordrecht: Springer Science + Business Media, pp. 31–46.

European Centre for Medium-Range Weather Forecasts. (2009) *ERA-Interim Project*. Research Data Archive at the National Center for Atmospheric Research. Boulder, CO: Computational and Information Systems Laboratory. Available at: http://rda.ucar.edu/datasets/ds627.0 (Accessed 29th November 2018).

Frakes, B. and Yarnal, B. (1997) A procedure for blending manual and correlation-based synoptic classifications. *International Journal of Climatology*, 17, 1381–1396.

Ganor, E., Osetinsky, I., Stupp, A. and Alpert, P. (2010a) Increasing trend of African dust, over 49 years, in the eastern Mediterranean. *Journal of Geophysical Research*, 115, D07201.

Ganor, E., Stupp, A., Osetinsky, I. and Alpert, P. (2010b) Synoptic classification of lower troposphere profiles for dust days. *Journal of Geophysical Research*, 115, D11201.

Gasch, P., Rieger, D., Walter, C., Khain, P., Levi, Y., Knippertz, P. and Vogel, B. (2017) Revealing the meteorological drivers of the September 2015 severe dust event in the eastern Mediterranean. *Atmospheric Chemistry and Physics*, 17, 13573–13604.

Goldreich, Y. (2003) *The Climate of Israel: Observation, Research and Application*. Israel/Netherlands: Springer/Kluwer Academic/Plenum Publishers.

Hochman, A., Harpaz, T., Saaroni, H. and Alpert, P. (2018a) Synoptic classification in 21st century CMIP5 predictions over the eastern Mediterranean with focus on cyclones. *International Journal of Climatology*, 38, 1476–1483.

Hochman, A., Harpaz, T., Saaroni, H. and Alpert, P. (2018b) The seasons' length in 21st century CMIP5 projections over the eastern Mediterranean. *International Journal of Climatology*, 38, 2627–2637.

Kahana, R., Ziv, B., Enzel, Y. and Dayan, U. (2002) Synoptic climatology of major floods in the Negev desert, Israel. *International Journal of Climatology*, 22, 867–882.

Kalnay, E., Kanamitsu, M., Kistler, R., Collins, W., Deaven, D., Gandin, L., Iredell, M., Saha, S., White, G., Woollen, J., Zhu, Y., Leetmaa, A., Reynolds, R., Chelliah, M., Ebisuzaki, W., Higgins, W., Janowiak, J., Mo, K.C., Ropelewski, C., Wang, J., Jenne, R. and Joseph, D. (1996) The NCEP/NCAR 40-year reanalysis project. *Bulletin of the American Meteorological Society*, 77, 437–471.

Kistler, R., Kalnay, E., Collins, W., Saha, S., White, G., Woollen, J., Chelliah, M., Ebisuzaki, W., Kanamitsu, M., Kousky, V., van den Dool, H., Jenne, R. and Fiorino, M. (2001) The NCEP-NCAR 50-year reanalysis: monthly means CD-ROM and documentation. *Bulletin of the American Meteorological Society*, 82, 247–267.

Koplowitz, R. (1973) *An objective classification of synoptic pressure field patterns of the Eastern Mediterranean Basin for use in synoptic-climatological studies*. MSc Thesis, Jerusalem, The Hebrew University, Jerusalem.

Krichak, S.O., Alpert, P. and Krishnamurti, T.N. (1997a) Interaction of topography and tropospheric flow: a possible generator for the Red Sea trough? *Meteorology and Atmospheric Physics*, 63, 149–158.

Krichak, S.O., Alpert, P. and Krishnamurti, T.N. (1997b) Red Sea trough/cyclone development numerical investigation. *Meteorology and Atmospheric Physics*, 63, 159–170.

Krichak, S.O., Breitgand, J.S. and Feldstein, S.B. (2012) A conceptual model for identification of the active Red Sea trough synoptic events over southeastern Mediterranean. *Journal of Applied Meteorology and Climatology*, 51(5), 962–971.

Lionello, P. (Ed.). (2012) *The Climate of the Mediterranean Region, From the past to the Future*. Amsterdam: Elsevier.

Pinto, J.G., Spangeh, T., Ulbrich, U. and Speth, P. (2005) Sensitivities of a cyclone detection and tracking algorithm: individual tracks and climatology. *Meteorologische Zeitschrift*, 14, 823–838.

Romem, M., Ziv, B. and Saaroni, H. (2007) Scenarios in the development of Mediterranean cyclones. *Advances in Geosciences*, 12, 59–65.

Ronberg, B. (1984) *An objective weather typing system for Israel: a synoptic climatological study*. PhD Thesis, Jerusalem, Hebrew University.

Saaroni, H., Bitan, A., Alpert, P. and Ziv, B. (1996) Continental polar outbreaks into the eastern Mediterranean. *International Journal of Climatology*, 16, 1175–1191.

Saaroni, H., Ziv, B., Bitan, A. and Alpert, P. (1998) Easterly wind storms over Israel. *Theoretical and Applied Climatology*, 59, 61–77.

Saaroni, H., Ziv, B., Osetinsky, I. and Alpert, P. (2010a) Factors governing the inter-annual variation and the long-term trend of the 850-hPa temperature over Israel. *Quarterly Journal of the Royal Meteorological Society*, 136, 305–318.

Saaroni, H., Ziv, B. and Uman, T. (2010b) Does a synoptic classification indicate the $NO_x$ pollution potential? The case of the metropolitan area of Tel-Aviv, Israel. *Water, Air, and Soil Pollution*, 207, 139–155.

Shafir, H., Ziv, B., Neeman, B.U. and Alpert, P. (1994) Objective classification of synoptic situations and its implication for economic evaluation of wind energy availability. *Meteorologia be-Israel*, 3, 29–49 (in Hebrew).

Solot, S.B. (1950) General circulation over the Anglo-Egyptian Sudan and adjacent regions. *Bulletin of the American Meteorological Society*, 31, 85–94.

Tsvieli, Y. and Zangvil, A. (2005) Synoptic climatological analysis of "wet" and "dry" Red Sea troughs over Israel. *International Journal of Climatology*, 25, 1997–2015.

Tsvieli, Y. and Zangvil, A. (2007) Synoptic climatological analysis of Red Sea trough and non-Red Sea trough rain situations over Israel. *Advances in Geosciences*, 12, 137–143.

Uppala, S.M., Kållberg, P., Simmons, A.J., Andrae, U., Bechtold, P., Fiorino, M., Gibson, J.K., Haseler, J., Hernandez, A., Kelly, G. A., LI, X., Onogi, K., Saarinen, S., Sokka, N., Allan, R.P., Andersson, E., Arpe, K., Balmaseda, M.A., Beljaars, A.C.M., van de Berg, L., Bidlot, J., Bormann, N., Caires, S., Chevallier, F., Dethof, A., Dragosavac, M., Fisher, M., Fuentes, M., Hagemann, S., Hólm, E.V., Hoskins, B.J., Isaksen, L., Janssen, P.A.E.M., Jenne, R., cNally, A.P., Mahfouf, J.-F., Morcrette, J.-J., Rayner, N.A., Saunders, R.W., Simon, P., Sterl, A., Trenberth, K.E., Untch, A., Vasiljevic, D., Viterbo, P. and Woollen, J. (2005) The ERA-40 re-analysis. *Quarterly Journal of the Royal Meteorological Society*, 131(612), 2961–3012.

Ziv, B., Dayan, U. and Sharon, D. (2005) A mid-winter, tropical extreme flood-producing storm in southern Israel: synoptic scale analysis. *Meteorology and Atmospheric Physics*, 69, 91–102.

Ziv, B., Harpaz, T. and Saaroni, H. (2015) A new methodology for identifying daughter cyclogenesis - application for the Mediterranean Basin. *International Journal of Climatology*, 35(13), 3847–3861.

**How to cite this article:** Saaroni H, Harpaz T, Alpert P, Ziv B. Automatic identification and classification of the northern part of the Red Sea trough and its application for climatological analysis. *Int J Climatol*. 2020;40:3607–3622. https://doi.org/10.1002/joc.6416